DOI: https://doi.org/10.51922/2616-633X.2023.7.2.2033

TELLURIUM-BASED CHITOSAN HYDROGEL AS AN EFFICIENT NIR-INDUCED ANTIBACTERIAL PLATFORM

Li Leijiao[1,2], L. Shestakova[3], Jianxun Ding[4], Tianmeng Sun[5], Wenliang Li[1,2], Yu. Ostrovsky[3]

Changchun University of Science and Technology, Changchun, P. R. China[1]
Zhongshan Institute, Changchun University of Science and Technology, Zhongshan, P. R. China[2]
Belarusian State Scientific and Practical Center of Cardiology, Minsk, Belarus[3]
Changchun Institute of Applied Chemistry, Chinese Academy of Sciences, Changchun, P. R. China[4]
Key Laboratory of Organ Regeneration and Transplantation of Ministry of Education, Institute of Immunology, The First Hospital, Jilin University, Changchun, P. R. China[5]
yoryost@yaho.com, shestakova@hotmail.com

УДК 612.17:615.281:577.1

Key words: *tellurium nanoparticles (Te NPs), chitosan hydrogel (CS), antibacterial platform CS/TE.*

FOR REFERENCES. Li Leijiao, L. Shestakova, Jianxun Ding, Tianmeng Sun, Wenliang Li, Yu. Ostrovsky. Tellurium-based chitosan hydrogel as an efficient NIR-induced antibacterial platform. *Neotlozhnaya kardiologiya i kardiovaskulyarnye riski* [Emergency cardiology and cardiovascular risks], 2023, vol. 7, no. 2, pp. 2033–2040.

A kind of butterfly-shaped tellurium nanoparticles (Te NPs) is prepared in this paper, which have good biocompatibility, their uniform size is about 200 nm, and their photothermal conversion efficiency (η) is as high as 52.9%. Subsequently, a bidirectional freezing method was used to prepare a chitosan hydrogel (CS) with a sponge-like structure, which has excellent porosity and solubility. Its porosity exceeds 75% and can maintain a moisturizing effect for about 16 hours. Then, the prepared Te NPs were introduced into CS to construct a CS/Te antibacterial platform, which was effective against Staphylococcus aureus (S. aureus) and Escherichia coli (E. coli). These results suggested that CS/Te antibacterial platform could be a promising NIR light-activated antibacterial candidate material for biomedical applications.

ГИДРОГЕЛЬ НА ОСНОВЕ ХИТОЗАНА И НАНОЧАСТИЦ ТЕЛЛУРА (CS/TE) – ОСНОВНЫЕ ХАРАКТЕРИСТИКИ И ПЕРСПЕКТИВЫ ПРИМЕНЕНИЯ НОВОЙ ЭФФЕКТИВНОЙ АНТИБАКТЕРИАЛЬНОЙ ПЛАТФОРМЫ

Ли Лейцзяо[1,2], Л. Шестакова[3], Цзяньсунь Дин[4], Тяньмэн Сун[5], Вэньлян Ли[1,2], Ю. Островский[3]

Чанчуньский университет науки и техники, Чанчунь, КНР[1]
Чжуншаньский институт, Чанчуньский университет науки и техники, Чжуншань, КНР[2]
Республиканский научно-практический центр «Кардиология»,Минск, Беларусь[3]
Чанчуньский институт прикладной химии Академии наук Китая, Чанчунь, КНР[4]
Лаборатория регенерации и трансплантации органов Министерства образования, Институт иммунологии, Первая больница, Цзилиньский университет, Чанчунь, КНР[5]

Ключевые слова: *наночастицы теллура, гидрогель на основе хитозана, антибактериальный материал хитозан/теллур (CS/TE).*

ДЛЯ ЦИТИРОВАНИЯ. Ли Лейцзяо, Л. Шестакова, Цзяньсунь Дин, Тяньмэн Сун, Вэньлян Ли, Ю. Островский. Гидрогель на основе хитозана и наночастиц теллура (CS/TE) – основные характеристики и перспективы применения новой эффективной антибактериальной платформы. *Неотложная кардиология и кардиоваскулярные риски*, 2023, Т. 7, № 2, С. 2033–2040.

Появление устойчивости к антибиотикам потребовало разработки новых противомикробных методов лечения. Согласно описанным в литературе данным, композиты полимер-металл демонстрируют антибактериальную и антибиопленочную активность против E. Coli и S. Enterica. Кроме того, наночастицы теллура (Te NPs) обладают значительной активность по улавливанию свободных радикалов ABTS и DPPH, демонстрируют цитотоксичность в отношении раковых клеток (A549 и PC3) по сравнению с нормальными клетками (клетками NIH3T3).

В этой статье описан процесс получения наночастиц теллура в форме бабочки, которые обладают хорошей биосовместимостью. Их однородный размер составляет около 200 нм, а эффективность их фототермического преобразования (η) достигает 52,9%. Для получения гидрогеля хитозана (CS / ГХ) с губчатой структурой, обладающего превосходной пористостью и растворимостью, был использован метод двунаправленного замораживания. Пористость субстрата превышает 75% и может сохранять увлажняющий эффект около 16 часов. Подготовленные наночастицы теллура вводили в гидрогель хитозана для создания антибактериальной платформы CS/Te, которая продемонстрировала эффективность против золотистого стафилококка (S. Aureus) и кишечной палочки (E. Coli).

Приведенные результаты позволяют предположить, что антибактериальная платформа CS/Te может стать перспективным антибактериальным материалом, для биомедицинских применений.

Skin is considered the most important organ of the human body. It not only provides stimulation and perception, but also promotes material exchange and maintains health [1–3]. However, skin trauma can occur in almost any process, such as accidents, surgical treatments, diseases, etc [4]. At present, about 100 million wounds are treated in China every year, and with the aging of the population, this number is still increasing. In particular, the treatment of bacterial infections in clinical postoperative wounds is still one of the problems that needs to be solved urgently [5–10]. The development of photothermal therapy (PTT) offers exciting possibilities for future advanced antibacterial strategies because of its high precision, controllability, noninvasiveness, and broad-spectrum antibacterial activity [11]. More importantly, PTT could kill bacteria by directly destroying the structure rather than participating in metabolism, and almost does not produce drug resistance [12]. These satisfactory properties suggest that PTT may be an alternative to antibiotics and is expected to become a next-generation antibacterial strategy. In order to protect the wound and accelerate the healing process, various types of wound dressings have been developed, including gauze, cotton wool, plaster, hydrogel, polymer film, etc. [13–17]. Among them, hydrogels are becoming the most competitive candidate materials for the next generation of wound dressings due to their advantages such as high-water content, good biocompatibility, and a 3D porous structure similar to extracellular matrix [18–22]. Usually, the realization of PTT relies on photothermal agents (PTAs), which convert light into heat [23]. In order to avoid the aggregation and potential toxicity of PTAs, they are usually incorporated into suitable carriers, especially in wound treatment applications. Hydrogels with a three-dimensional porous structure can effectively immobilize PTAs to form composite hydrogels, which could be beneficial to promote wound healing [24]. Therefore, we constructed a composite hydrogel antibacterial nanoplatform based on CS and Te NPs, and evaluated the antibacterial activity of the hydrogel.

We first synthesized tellurium nanoparticles (Te NPs) by reference to the preparation of homologous Te NPs [25]. The specific preparation method is as follows: 0.2 mmol Na_2TeO_3, 5 mmol KBr, 0.1 g PVP, 0.4 mmol ascorbic acid add to the 50 mL round-bottomed flask and incubate for 3 h at 80 °C. Wash three times with water and ethanol to obtain Te NPs, which are stored in a refrigerator at 4 °C for subsequent use. Figure 1a shows transmission electron microscopy (TEM) images of Te NPs, from which it can be seen that the Te NPs are butterfly shaped and well dispersed with a uniform size of about 200 nm and 60 nm cross-section. Figure 1b shows an X-ray diffraction (XRD) pattern of the Te NPs, matching the standard card PDF#78-2312, indicating good crystallinity and the material's relatively complete morphological structure. The X-ray photon spectra (XPS) of Te NPs show the presence of the element Te, providing evidence that the synthesized nanomaterials are Te NPs (Figure 1c-d). The ultraviolet-visible spectroscopy (UV-vis) spectra of Te NPs at different concentrations are shown in Figure 1d. The water, PBS and LB medium solution of Te NPs remain stable after 7 days (Figure e-j).

The synthesized Te NPs have good NIR absorption and the photothermal effect was evaluated. Aqueous solutions of Te NPs with different concentrations were placed under an NIR light source (808 nm, 2 W cm^{-2}) to observe the temperature rise within 10 min. The Te NPs showed an excellent warming effect and a strong concentration-dependent photothermal effect compared with water (Fig. 2a, c). The UV-vis spectra of Te NPs showed negligible change before and after irradiation (Figure 2b). There was no significant decrease in the warming effect after four cycles, indicating the good photothermal stability of Te NPs (Fig. 2d). The photo-thermal conversion efficiency (h) of Te NPs was 52.9% calculated from Figure 2e-f. These results suggested that the synthesized Te NPs have good photothermal properties [26, 27].

Subsequently, we used the bidirectional freezing method to prepare a CS/Te NPs hydrogel with regular internal pore structure and uniform growth direction [28]. The absorption capacity of this hydrogel is better than that prepared by conventional freezing method. The pore structure is conducive to absorbing exudate from

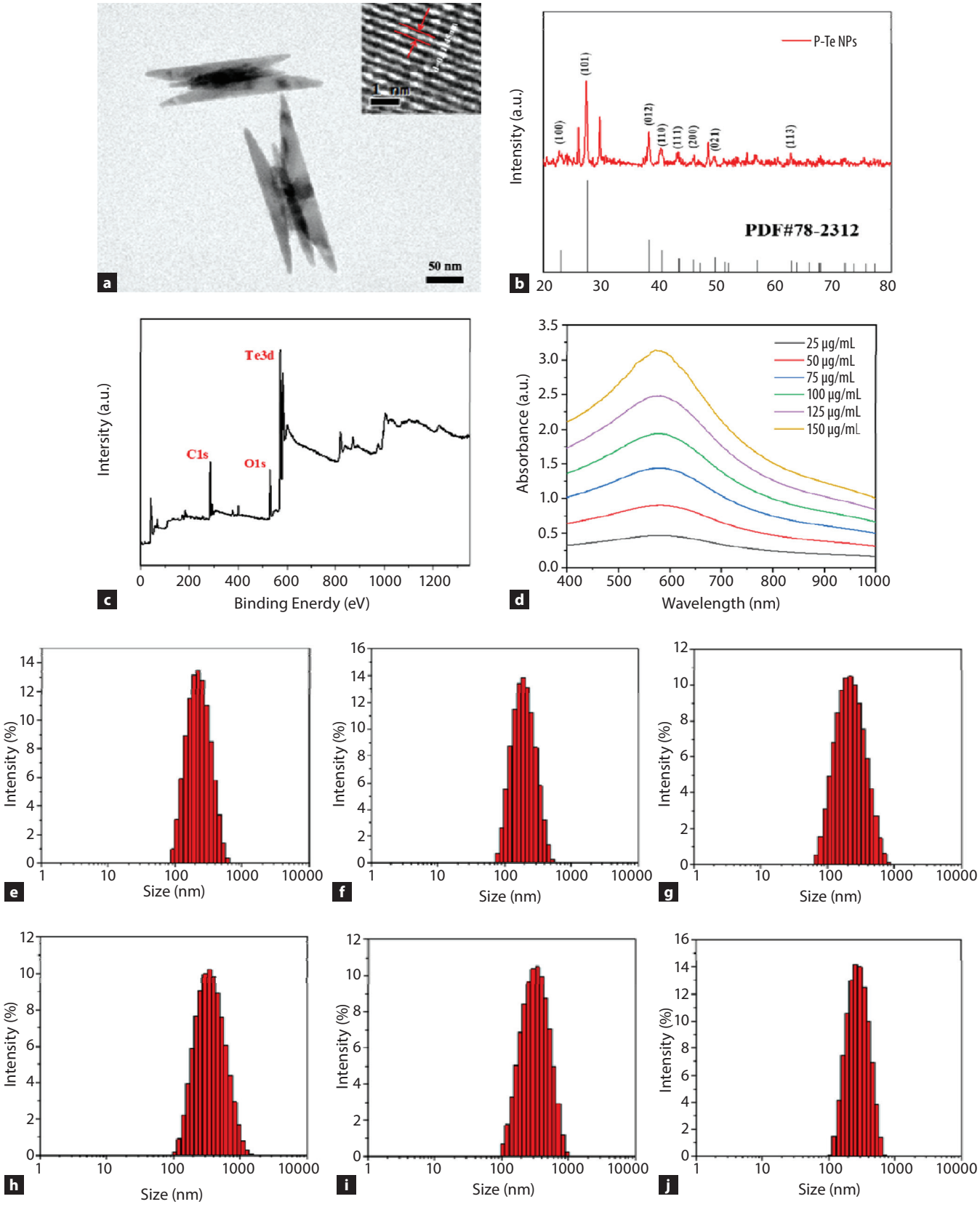

Figure 1. Characterization of Te NPs. (a) TEM and HRTEM images (b) XRD pattern (c) XPS pattern (d) UV-vis spectra of Te NPs at different concentration. (e-j) hydrodynamic diameters of Te NPs deionized water solution for different times, (e-g): 0 days; (h-j): 7 days

Рисунок 1. Характеристика наночастиц теллура. (a) изображения TEM и HRTEM (b) модель XRD (c) модель XPS (d) УФ-спектры наночастиц теллура при различной концентрации (e-j) гидродинамические диаметры раствора наночастиц теллура в деионизированной воде за разное время, (e-g): 0 дней; (h-j): 7 дней

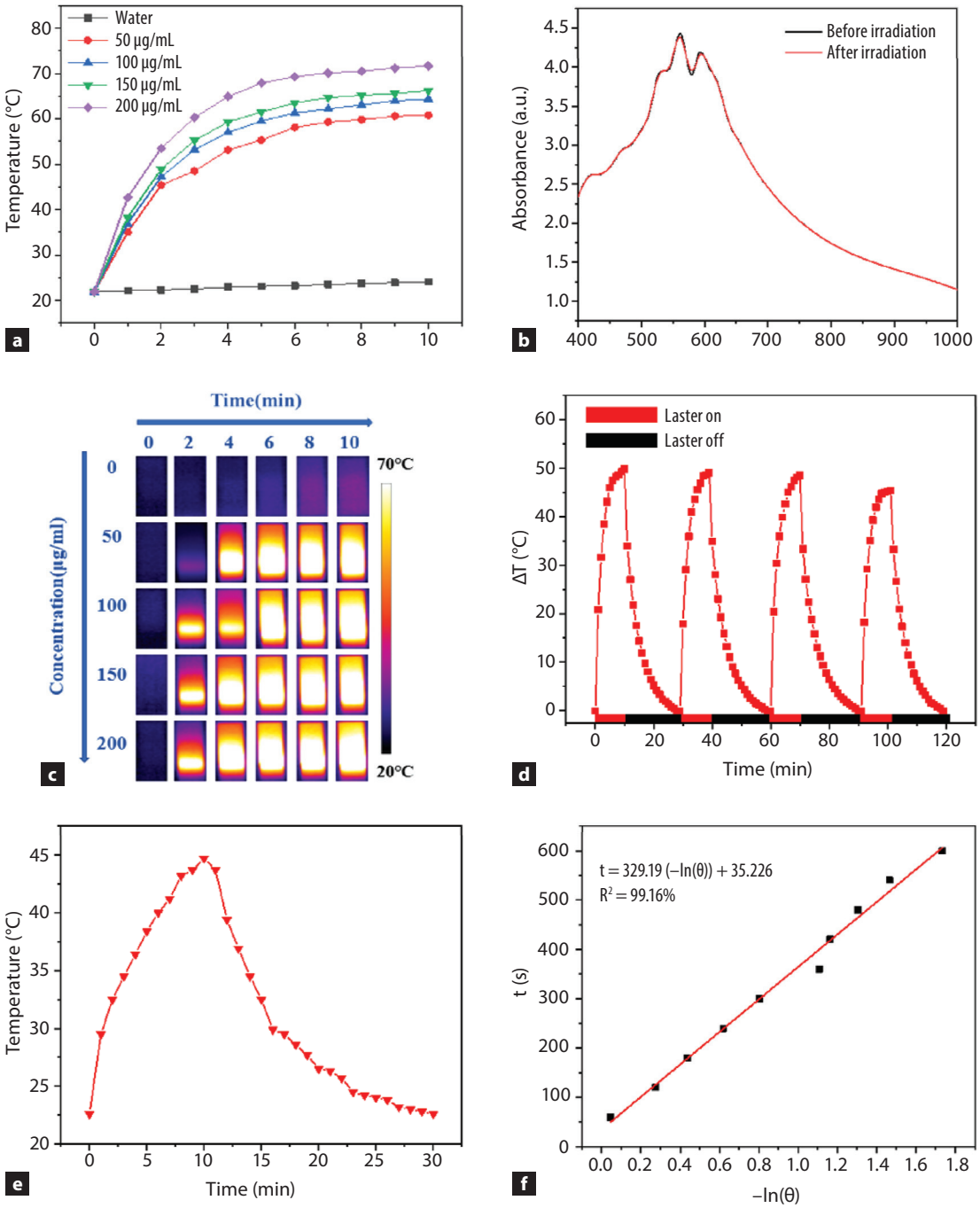

Figure 2. The photothermal heating effect of Te NPs. (a) photothermal heating curves and infrared thermal images under NIR irradiation (808 nm, 1.5 W cm^{-2}). (b) the absorption of Te NPs before and after irradiation. (c) photos of infrared thermography (d) heating and cooling cycles at Te NPs. (e) cooling curve of Te NPs. (f) The plot of cooling time t versus -ln(θ)

Рисунок 2. Эффект фототермического нагрева наночастиц теллура. (а) кривые фототермического нагрева и тепловые изображения в инфракрасном диапазоне при облучении NIR (808 нм, 1,5 Вт $см^{-2}$). (б) поглощение наночастиц теллура до и после облучения. (c) фотографии инфракрасной термографии (d) циклы нагрева и охлаждения у наночастиц теллура. (e) кривая охлаждения наночастиц теллура. (f) График зависимости времени охлаждения t от -ln(θ)

the wound surface. Figure 3a-e shows the internal structure of CS hydrogel compounded with Te NPs at different concentrations (0.05 mg/mL, 0.1 mg/mL, 0.15 mg/mL, 0.2 mg/mL, CS/Te^{x}, x = 0, 0.05, 0.1, 0.15, 0.2). Hydrogel is composed of neatly ordered and well-connected pores with a pore diameter of 100~300 μm. Figure 3f and g were the SEM image of CS/$Te^{0.2}$ hydrogel. It could be seen that Te NPs were well dispersed in the CS hydrogel skeleton. The element mapping in Figure 3h showed the uniform distribution of C, O, and Te in CS/$Te^{0.2}$ hydrogel. Figure 3i showed the porosity of CS/Te NPs hydrogels with five concentrations. Even after adding

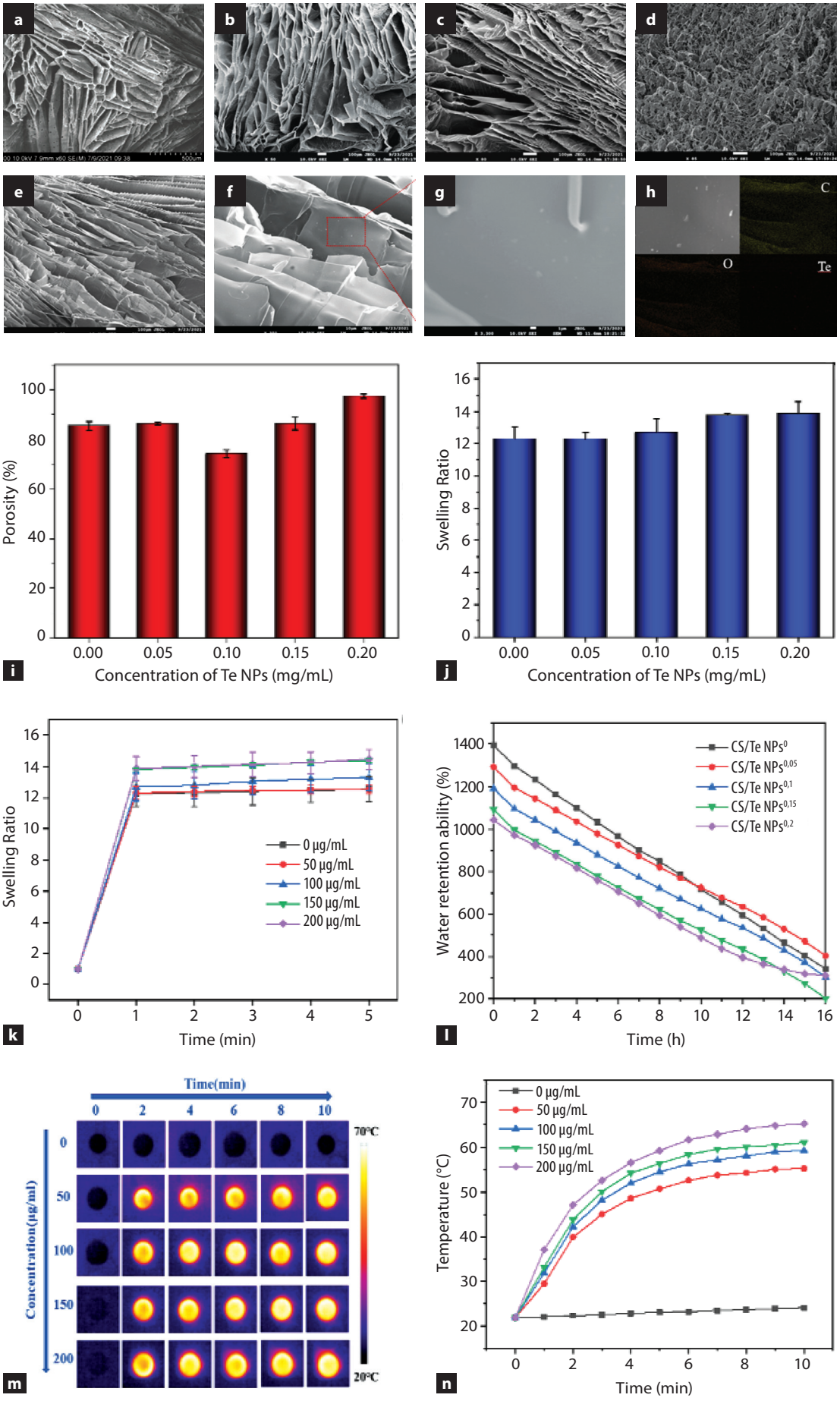

Figure 3. Characterization of CS/Te hydrogels. (a) CS/Te NPs^{0} hydrogel, scale bar: 500 μm. (b) CS/Te NPs$^{0.05}$ hydrogel, scale bar: 100 μm. (c) CS/Te NPs$^{0.1}$ hydrogel, scale bar: 100 μm. (d) CS/Te NPs$^{0.15}$ hydrogel, scale bar: 100 μm. (e) CS/Te NPs$^{0.2}$ hydrogel, scale bar: 100 μm. (f-g) partial enlargement of CS/Te NPs$^{0.2}$ hydrogel, scale bars: 10 and 1 μm. (h) EDS spectra and element mapping images for O, C and Te in CS/Te NPs$^{0.2}$ hydrogel. (i) porosity (j) water absorbency (k) swelling ratio (l) moisturizing change curve (m) photos of infrared thermography (n) temperature changes with the increasing irradiation time

Рисунок 3. Характеристика гидрогелей CS/Te. (a) Гидрогель CS/Te NPs^{0}, шкала: 500 мкм. (b) Гидрогель CS/Te NPs$^{0.05}$, шкала: 100 мкм. (c) Гидрогель CS/Te NPs$^{0.1}$, шкала: 100 мкм. (d) Гидрогель CS/Te NPs$^{0.15}$, шкала: 100 мкм. (e) гидрогель CS/Te NPs$^{0.2}$, шкала: 100 мкм. (f-g) частичное увеличение гидрогеля CS /Te NPs$^{0.2}$, шкалы: 10 и 1 мкм. (h) Спектры EDS и изображения картирования элементов для O, C и Te в гидрогеле CS/Te NPs$^{0.2}$. (i) пористость (j) водопоглощающая способность (k) коэффициент набухания (l) кривая изменения влажности (m) фотографии инфракрасной термографии (n) изменения температуры с увеличением времени облучения

Te NPs, all CS/Te NPs hydrogels showed the same porosity (75~97%). The highly porous nature of CS/Te NPs hydrogel helped absorb a large amount of wound exudate from the wound surface. In addition, the porosity was conducive to gas exchange and was beneficial to wound healing. Figure 3j showed the water absorption analysis of CS/Te NPs hydrogel. Its water absorption was 6 times and 3 times that of cotton and gauze commonly used in the market, respectively. After loading Te NPs, the water absorption of CS/Te NPs hydrogel did not decrease. Figure 3k showed the swelling rate diagram of CS/Te hydrogel. The test results showed that the swelling ratios of blank CS hydrogel and CS/Te$^{0.2}$ hydrogel were both in the range of 12 to 14, and their swelling ratios increase over time. It was found that CS/Te hydrogel has a high swelling capacity and could absorb wound permeate for a long time. Compared with traditional dressings such as cotton and gauze, CS/Te has superior performance. Figure 3m-n showed the change curve of CS/Te hydrogel temperature with 808 nm laser irradiation time. As the Te NPs content increased, the maximum temperature in the core region of CS/Te NPs hydrogel increased significantly. When the concentration of Te NPs was 200 μg/mL, the temperature of the CS/Te 0.2 hydrogel increased to 65.2 °C after irradiation for 10 min.

Finally, we used the plate counting method to explore the *in vitro* antibacterial effect of CS/Te hydrogel on Gram-positive bacteria Escherichia coli (E. coli) and Gram-negative bacteria Staphylococcus aureus (S. aureus). E. coli and S. aureus were used to evaluate the *in vitro* bactericidal effect of CS/Te hydrogels. First, 500 mL of bacterial suspension and 500 mL of CS/Te hydrogels were mixed. The bacterial suspension was 10^8 CFU mL^{-1} (OD600 0.5) and the CS/Te

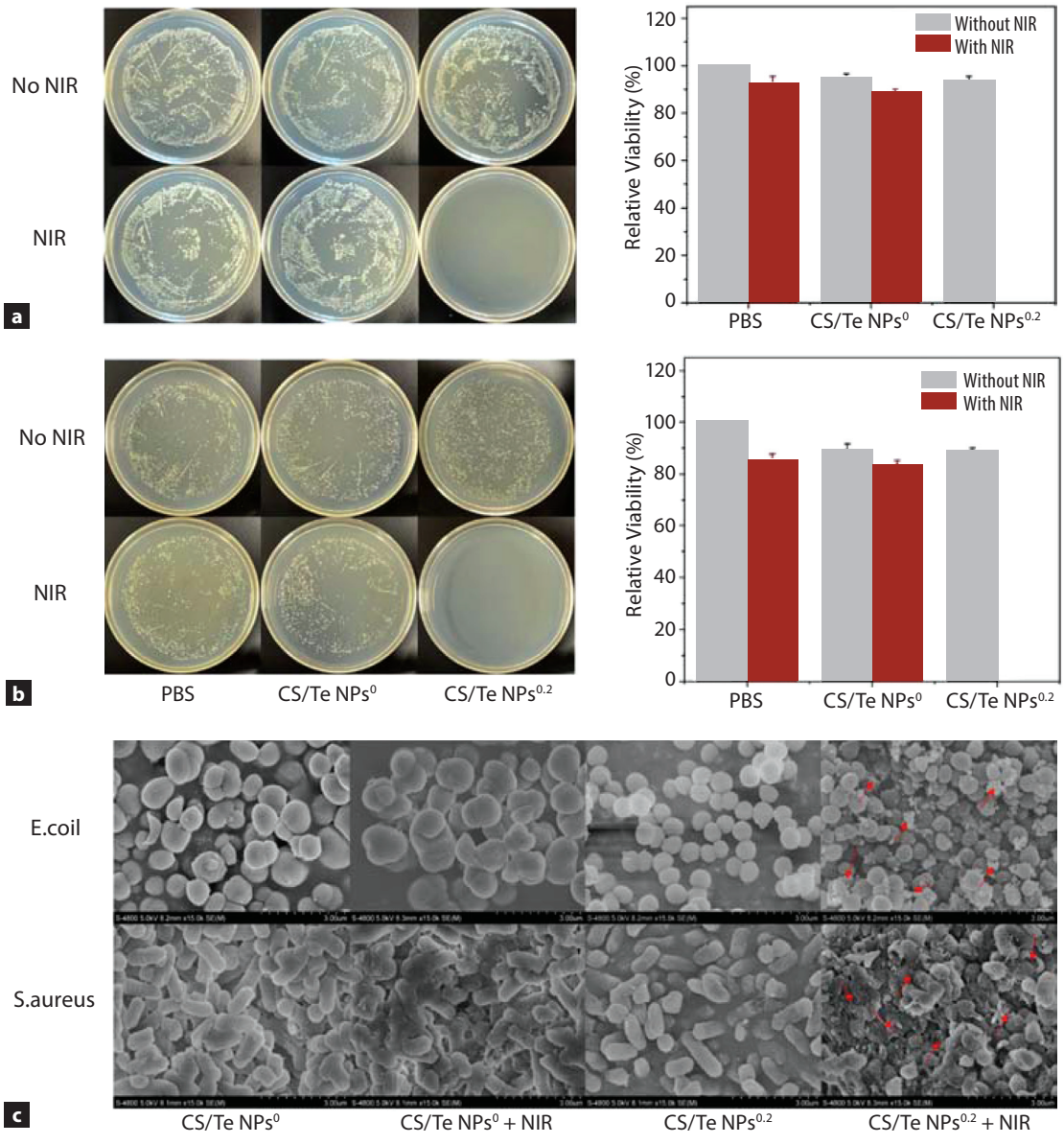

Figure 4.
In vitro antibacterial activity of CS/Te.
(a) E. coli colony photographs and data statistics of PBS, CS/Te NPs^0 and CS/Te NPs$^{0.2}$ under 808 nm laser irradiation (1.5 W cm^{-2}, 10 min).
(b) S. aureus colony photographs and data statistics were obtained for PBS, CS/Te NPs^0 and CS/Te NPs$^{0.2}$ under 808 nm laser irradiation (1.5 W cm^{-2}, 10 min).
(c) the SEM pictures of bacteria after different treatments

Рисунок 4.
Антибактериальная активность CS/Te in vitro. (a) Фотографии колоний E. coli и статистика данных PBS, CS/Te NPs^0 и CS/Te NPs$^{0.2}$ при облучении лазером с длиной волны 808 нм (1,5 Вт см$^{-2}$, 10 мин).
(b) Фотографии колоний S. aureus и статистические данные были получены для PBS, CS/Te NPs^0 и CS/Te NPs$^{0.2}$ при облучении лазером с длиной волны 808 нм (1,5 Вт см$^{-2}$, 10 мин).
(c) СЭМ-изображения бактерий после различных обработок

hydrogels concentration was 50 mg mL^{-1}. The mixture was incubated at 37 °C for 2 h and irradiated (808 nm 1.5 W cm^{-2}) for 10 min. PBS were used as controls. Bacteria treated in different ways grew on solid culture media. The number of colonies that emerged intuitively reflects the antibacterial performance of the CS/Te hydrogel. Figure 4a shows the results of E. coli and Vitis vinifera under near-infrared laser irradiation (1.5 W/cm^2, 808 nm), with PBS as the blank control group, CS/Te^0 hydrogel and CS/$Te^{0.2}$ hydrogel as the treatment groups. The experimental results showed that there was no significant difference between the PBS-treated group and the PBS+NIR-treated group, indicating that the use of NIR laser alone cannot effectively inhibit the growth of bacteria. As shown in Figure 4a, the lethality rates of the CS/Te^0 hydrogel non-illuminated group and the illuminated group against E. coli were 4.9% and 11.2%, respectively. It showed that chitosan possessed inhibitory effects on bacteria. However, the lethality rates of CS/$Te^{0.2}$ hydrogel against E. coli in the non-illuminated groups and illuminated groups were 6.3% and 100%, indicating that CS/$Te^{0.2}$ hydrogel have good antibacterial ability. Similarly, the lethality rates of the CS/Te NPs^0 hydrogel non-illuminated group and the illuminated group against S. aureus were 10.7% and 16.3%, respectively. However, the lethality rates of CS/$Te^{0.2}$ hydrogel against S. aureus were 6.3% and 100% for without laser group and with laser group, indicating that CS/$Te^{0.2}$ hydrogel have good antibacterial ability. To further investigate the antibacterial mechanism of CS/Te hydrogel, the cell morphology of bacteria after CS/Te treatment was observed by scanning electron microscope (SEM). As can be seen in Figure 4c, the growth status of bacteria in the PBS control group was well maintained, so that the bacterial morphology was uniform and plump, while both bacterial surfaces in the CS/$Te^{0.2}$ + NIR experimental groups showed obvious wrinkling or rupture, so that the cell integrity was significantly impaired. An excellent sterilization effect from the treatment was obtained as expected. It is speculated that the antibacterial mechanism may be that CS/Te hydrogel, which is distributed near the bacterial cell wall and cell membrane, rapidly heats up under irradiation from a near-infrared laser. High temperature could directly damage the bacterial cell wall and membrane system, release the bacterial cytoplasmic matrix, affect its metabolism, and lead to the death of the bacteria.

In summary, the butterfly-shaped Te NPs with a quite high photothermal conversion efficiency of 52.9% were obtained by one-pot method. Then Te NPs were loaded onto CS hydrogel to create a NIR-induced therapeutic antibacterial platform (CS/Te). The CS/Te platform could rapidly kill bacteria including Gram-negative and Gram-positive bacteria under 808 nm NIR irradiation. We hope this work could provide a new material or strategy for the treatment of bacterial infections.

Conflicts of interest
There are no conflicts to declare.

Acknowledgements
This work was partially financially supported by the Science and Technology Research Project of Jilin Education Bureau (No. JJKH20230804KJ).

REFERENCES

1. E M Tottoli, R Dorati, I Genta, et al. Skin Wound Healing Process and New Emerging Technologies for Skin Wound Care and Regeneration[J]. Pharmaceutics, 2020(8): 735.
2. S Kirchner, V Lei, A S MacLeod. The Cutaneous Wound Innate Immunological Microenvironment[J]. International Journal of Molecular Sciences, 2020, 21(22): 8748.
3. Lu Huidan, Tu Chenxi, Zhou Tong, et al. A ROS-scavenging hydrogel loaded with bacterial quorum sensing inhibitor hyperbranched poly-L-lysine promotes the wound scar-free healing of infected skin in vivo[J]. Chemical Engineering Journal, 2022, 436: 135130.
4. M Bulut, A D Kucuk, A Bulut, et al. Evaluation of accidental and intentional pediatric poisoning: Retrospective analysis in an emergency Department of Turkey[J]. Journal of pediatric nursing care of Children&Families, 2022, 63: 44-49.
5. Yang Yuxuan, Zhao Xiaodan, Yu Jing, et al. Bioactive skin-mimicking hydrogel band-aids for diabetic wound healing and infectious skin incision treatment[J]. Bioactive Materials, 2021, 6(11): 3962-3975.
6. Xue Meilang, Zhao Ruilong, et al. Delivery systems of current biologicals for the treatment of chronic cutaneous wounds and severe burns[J]. Advanced Drug Delivery Reviews, 2018, 129: 219-241.
7. J Dissemond, M Romanelli. Inflammatory skin diseases and wounds[J]. British Journal of Dermatology, 2022, 187(2): 167-177.
8. S W Gerdin, A Lie, A Asarnoj, et al. Impaired skin barrier and allergic sensitization in early infancy[J]. Allergy, 2021, 77(5): 1464-1476.
9. S G Danby, P V Andrew, L J Kay, et al. Enhancement of stratum corneum lipid structure improves skin barrier function and protects against irritation in adults with dry, eczema-prone skin[J]. British Journal of Dermatology, 2022, 186(5): 875-886.
10. Zeng Qiankun, Qi Xiaoliang, Shi Guoyue, et al. Wound Dressing: From Nanomaterials to Diagnostic Dressings and Healing Evaluations[J]. ACS NANO, 2022, 16(2): 1708-1733.
11. Huo Jingjing, Jia Qingyan, Huang Han, et al. Emerging photothermal-derived multimodal synergistic therapy in combating bacterial infections[J]. Chemical Society Reviews, 2021, 50(15): 8762-8789.
12. Xi Dongmei, Xiao Ming, Cao Jianfang, et al. NIR Light-Driving Barrier-Free Group Rotation in Nanoparticles with an 88.3% Photothermal Conversion Efficiency for Photothermal Therapy[J]. Advanced Materials, 2020, 32(11): 19078551.
13. A S Montaser, M Rehan, W M El-Senousy, et al. Designing strategy for coating cotton gauze fabrics and its application in wound healing[J]. Carbohydrate Polymers, 2020, 244: 116479.
14. A Abedin-Do, Zhang Ze, Y Douville, et al. Electrical stimulation promotes the wound-healing properties of diabetic human skin fibroblasts[J]. Journal of Tissue Engineering and Regenerative Medicine, 2022, 16(7): 643-652.
15. Xu Xiaowen, V V Jerca, R Hoogenboom. Bioinspired double network hydrogels: From covalent double network hydrogels via hybrid double network hydrogels to physical double network hydrogels[J]. Materials Horizons, 2020, 8(4): 1173-1188.
16. Duan Yumeng, Li Kaiyue, Wang Huangwei, et al. Preparation and evaluation of curcumin grafted hyaluronic acid modified pullulan polymers as a functional wound dressing material[J]. Carbohydrate Polymers, 2020, 238: 116195.

17. S Peers, A Montembault, C Ladavière. Chitosan hydrogels for sustained drug delivery[J]. Journal of Controlled Release, 2020, 326: 150-163.
18. Liang Limei, Hou Tingting, Ouyang Qianqian, et al. Antimicrobial sodium alginate dressing immobilized with polydopamine-silver composite nanospheres[J]. Composites Part B Engineering, 2020, 188(3): 107877.
19. R B Alam, M H Ahmad, M R Islam. Effect of MWCNT nanofiller on the dielectric performance of bio-inspired gelatinbased nanocomposites[J]. RSC Advances, 2022, 12(23): 14686-149697.
20. Chen Xiangyan, Li Hongjin, Qiao Xiaoni, et al. Agarose oligosaccharide-silver nanoparticle- antimicrobial peptide-composite for wound dressing[J]. Carbohydrate Polymers, 2021, 269: 118258.
21. Zhao Decai, Wei Yanze, Jin Quan, et al. PEG-Functionalized Hollow Multishelled Structures with On-Off Switch and Rate-Regulation for Controllable Antimicrobial Release[J]. Angewandte Chemie-International Edition, 2022, 61(36): 202206807.
22. Yao Xiuxiu, Yang Baochan, Wang Shan, et al. A novel multifunctional FePt/BP nanoplatform for synergistic Photothermal/Photodynamic/Chemodynamic cancer therapies and Photothermal enhanced Immunotherapy[J]. Journal of Materials Chemistry B, 2020, 8(35): 8010-8021.
23. Zheng Bingde, Xiao Meitian. Polysaccharide-based hydrogel with photothermal effect for accelerating wound healing[J]. Carbohydrate Polymers, 2023, 299: 1200228.
24. Wang, Jianhao, Chen Xiaoyi, Zhao Yuan, et al. pH-Switchable Antimicrobial Nanofiber Networks of Hydrogel Eradicate Biofilm and Rescue Stalled Healing in Chronic Wounds[J]. ACS nano, 2019, 13(10): 11686-11697.
25. Li Jiuxing, Li Yingfu. One-pot high-yield synthesis of Pd nanocubes for Pd-Ir nanocube-based immunoassay of nucleocapsid protein from SARS-CoV-2[J]. Analytical and Bioanalytical Chemistry, 2021, 413(18): 4635-4644.
26. Yuwan Zhu, Mo Deng, Nannan Xu, Yingjun Xie, Xuewen Zhang, A Tumor Microenvironment Responsive Nanotheranostics Agent for Magnetic Resonance Imaging and Synergistic Photodynamic Therapy/Photothermal Therapy of Liver Cancer[J], Front. Chem., 2021, 9: 650899.
27. Xiaojun He, Lixiong Dai, Lisong Ye, Xiaoshuai Sun, Oben Enoch, Rongdang Hu, Xingjie Zan, Feng Lin and Jianliang Shen, A Vehicle-Free Antimicrobial Polymer Hybrid Gold Nanoparticle as Synergistically Therapeutic Platforms for Staphylococcus aureus Infected Wound Healing[J], Adv. Sci., 2022, 9(14): 2105223.
28. Liu Yingnan, Xiao Yaqing, Cao Yuanyuan, et al. Construction of Chitosan-Based Hydrogel Incorporated with Antimonene Nanosheets for Rapid Capture and Elimination of Bacteria[J]. Advanced Functional Materials, 2020, 30(35): 2003196.

Поступила: 05.12.2023